Low-Level Cloud Response to the Gulf Stream Front in Winter using CALIPSO

Jing-Wu Liu[1]
Physical Oceanography Laboratory, and Ocean–Atmosphere Interaction and Climate Laboratory, Ocean University of China, Qingdao, China

Shang-Ping Xie
Scripps Institution of Oceanography, University of California, San Diego, La Jolla, California;
International Pacific Research Center and Department of Meteorology, School of Ocean and Earth Science and Technology, University of Hawaii, Honolulu, USA;
Physical Oceanography Laboratory, and Ocean–Atmosphere Interaction and Climate Laboratory, Ocean University of China, Qingdao, China

Joel R. Norris
Scripps Institution of Oceanography, University of California, San Diego, La Jolla, California

Su-Ping Zhang
Physical Oceanography Laboratory, and Ocean–Atmosphere Interaction and Climate Laboratory, Ocean University of China, Qingdao, China

[1] *Corresponding author address*: Jing-Wu Liu, Physical Oceanography Laboratory, and Ocean-Atmosphere Interaction and Climate Laboratory, Ocean University of China, Qingdao, China, 238, Songling Road, Laoshan, Qingdao 266100, China.
E-mail: liujingwu@126.com

Abstract

A sharp sea surface temperature front develops between the warm water of the Gulf Stream and cold continental shelf water in boreal winter. This front has a substantial impact on the marine boundary layer. The present study analyzes and synthesizes satellite observations and reanalysis data to examine how the sea surface temperature front influences the three-dimensional structure of low-level clouds. Cloud-Aerosol Lidar and Infrared Pathfinder Satellite Observation (CALIPSO) captures a sharp low-level cloud transition across the Gulf Stream front, a structure frequently observed under the northerly condition. Low-level cloud top (< 4 km) increases by about 500 m from the cold to the warm flank of the front. The sea surface temperature front induces a secondary low-level circulation through sea level pressure adjustment with ascending motion over the warm water and descending motion over cold water. The secondary circulation further contributes to the cross-frontal transition of low-level clouds. Composite analysis shows that surface meridional advection over the front plays an important role in the development of the marine atmospheric boundary layer and low-level clouds. Under cold northerly advection over the Gulf Stream front, strong near-surface instability leads to a well-mixed boundary layer over the Gulf Stream, causing southward deepening of low-level clouds across the sea surface temperature front. Moreover, the front affects the freezing level by transferring heat to the atmosphere and therefore influences the cross-frontal variation of the cloud phase.

1. Introduction

The Gulf Stream is the strongest western boundary current in the ocean transporting heat from the tropics to higher latitudes. A sharp sea surface temperature (SST) front forms between the warm water of the Gulf Stream and cold continental shelf water. The Gulf Stream dramatically influences local weather phenomena. It releases a huge amount of heat to the atmosphere in winter (Bane and Osgood 1989), contributing to the explosive cyclogenesis (Sanders and Gyakum 1980; Sanders 1986). Synoptic rainbands are frequently observed along the Gulf Stream axis (Hobbs 1987), and lighting flashes are more frequent and stronger over the Gulf Stream (Biswas and Hobbs 1990).

Recent studies have shown that the Gulf Stream also markedly affects the regional climate. Warm SST produces frequent high surface winds (Sampe and Xie 2007), strong wind speed (O'Neill et al. 2010) and surface wind convergence (Chelton et al. 2004) over the Gulf Stream. Minobe et al. (2008) found that the surface wind convergence anchors a band of rain and upward motion in the annual mean that extends from the boundary layer to the upper troposphere. Minobe et al. (2010) subsequently examined the seasonal cycle of the atmospheric response and found a shallow heating mode of the atmosphere by the Gulf Stream in winter and a deep-heating mode in summer. Numerical models indicate that strong SST gradient results in a deeper marine atmospheric boundary layer (MABL) over the warm water and induces a secondary cross-frontal circulation within the MABL (Huang and Raman 1988; Wai and Stage 1989).

Low-level clouds play an important role in air-sea interaction since they reduce the

amount of solar radiation absorbed by the ocean (Wood 2012) and they vary in height and morphology with the stratification of the MABL (Norris 1998a; Tokinaga et al. 2009). The influence of the Gulf Stream on synoptic low-level clouds has been previously reported. Cloud bands often originate at the upwind flank of the Gulf Stream meanders (Young and Sikora 2003). Li et al. (2004) observed a cloud line along the Gulf Stream axis in a satellite image. Similarly, Tokinaga et al. (2009) observed a sharp transition in MABL clouds across the Kuroshio Extension front using laser ceilometers mounted on research vessels. One shortcoming of previous studies is that they were generally based on research cruises or a small number of satellite observations, and the response of low-level clouds to the Gulf Stream on climate time scales remains poorly understood.

The large-scale climatology of marine cloudiness has been previously studied using visual observations from volunteer observing ships. Klein and Hartmann (1993) found that seasonal and interannual variations of low-level stratiform clouds are related to lower-tropospheric static stability. Norris (1998b) studied the global distribution of low-level clouds according to morphological categories and found a north-to-south transition from stratocumulus to cumulus when winds flow equatorward in the Western Pacific. Minobe et al. (2010) showed that mid-level cloud occurrence is most frequent right over the Gulf Stream in winter based on the Atmospheric Infrared Sounder and the Advanced Microwave Sounding Unit. Previous climatological studies, however, suffered from coarse spatial resolution and cannot depict variations of low-level clouds across the narrow SST front (about 200-300-km wide).

The Cloud-Aerosol Lidar and Infrared Pathfinder Satellite Observation (CALIPSO) satellite was launched on April 28, 2006 by NASA and the French Agency CNES to study the impact of clouds and aerosols on the Earth's radiation budget and climate (Winker et al. 2009). A selective, iterated boundary location algorithm is used to detect cloud layers from the lidar backscatter signals (Vaughan et al. 2009). CALIPSO provides a cloud-layer product with high spatial resolution. In addition, CALIPSO flies in formation with other five satellites (including AMSR-E, CloudSat and Aqua) in the sun-synchronous "A-train" for coincident observations. The combination of the CALIPSO lidar, CloudSat radar and MODIS infrared radiometer (DARDAR) provides vertical slices of cloud phase properties along the A-train tracks (Delanoë and Hogan 2008).

Global and regional cloud structures have been investigated using CALIPSO and DARDAR. Nazaryan et al. (2008) studied the spatial and temporal variations of global cirrus based on CALIPSO. Bouniol et al. (2012) and Stein et al. (2011) studied the cloud structure in West Africa. Medeiros et al. (2010) found that the vertical distribution of low-level cloud height is consistent with observations from the Rain in Cumulus Over the Ocean field study. Thus, CALIPSO offers the capability of detecting the small-scale structure of clouds.

The present study focuses on how low-level clouds respond to the Gulf Stream from a climate perspective by analyzing CALIPSO and synthesizing other satellite observations and reanalysis data. This paper is the first systematic study of SST frontal effects on clouds with direct observations by a cloud-top height instrument in space.

Taking advantage of a high-resolution and multiyear record of observations, we investigate how low-level clouds vary across the SST front in winter. We also use ERA-Interim to examine the MABL structure corresponding to cross-frontal variations of low-level clouds. Since the direction of meridional surface winds is important for the low-level atmospheric stability, we apply composite analysis according to the surface meridional winds. Our results serve as a template to study cloud transition near other strong SST fronts.

2. Data

a. Temporal and spatial domains

We employ a suite of high-resolution satellite observations and reanalysis data during the 5 winters (December of 2006-10, January and February of 2007-11) when the observations of CALIPSO, CloudSat and AMSR-E overlap. The DJF climatology in the present study is defined as the average values during this period. Note that QuikSCAT is available from July 1999 to November 2009, and does not perfectly overlap with CALIPSO. We refer to QuikSCAT averaged in DJF between 1999 and 2009 as a climatology. The spatial domain of the composite analysis is roughly 30 – 50°N, 65 – 50°W where the Gulf Stream flows nearly eastward.

b. Satellite observations

We use the CALIPSO cloud layer product (http://www-calipso.larc.nasa.gov/;

128 Winker et al. 2009) to investigate low-level cloud structure. Details on the retrieval
129 algorithms can be found in Vaughan et al. (2009). The spatial resolution of the CALIPSO
130 cloud layer product is 1 km in the horizontal and 30 m in the vertical below 8.5 km.
131 CALIPSO provides up to ten cloud-top heights per profile, and the highest cloud tops
132 below 4 km are considered to be the low-level cloud top (LCT) following the algorithm
133 of Zhang et al. (2012), who investigated cloud top heights near Hawaii. It should be noted
134 that CALIPSO observes low-level clouds only when the higher-clouds are not optically
135 thick. This is not a problem for the present study because low-level clouds are dominant
136 near the Gulf Stream in winter (not shown). Since this paper focuses on marine clouds,
137 CALIPSO profiles over land are omitted. CALIPSO passes the Gulf Stream region
138 around 0500 and 1600 UTC (0000 and 1100 in local time). Orbital tracks pass over the
139 same location at the same local time every 16 days.

140 We also use the DARDAR-MASK that combines CloudSat, CALIPSO and MODIS
141 (http://www.icare.univ-lille1.fr/projects/dardar/; Delanoë and Hogan 2010) examine the
142 cloud phase properties. The DARDAR-MASK returns a range of cloud categories: rain,
143 supercooled liquid water, liquid water, ice, and mixed ice and supercooled liquid. The
144 resolution of DARDAR-MASK is 1.5 km in the horizontal and 240 m in the vertical. We
145 use DARDAR-MASK data to investigate the occurrence of the different cloud categories
146 in the Gulf Stream region. Delanoë et al. (2013) compared airborne in situ, airborne
147 radar–lidar, and DARDAR retrievals of polar ice cloud properties and found that the
148 combination of radar and lidar provides better retrievals than do stand-alone methods

149 using just the lidar or radar. Further validation of DARDAR with direct measurements
150 would help reduce the uncertainties of DARDAR.

151 The AMSR-E sensor on the Aqua satellite measures SST, surface wind speed, liquid
152 water path (LWP, vertically integrated atmospheric water vapor) and rain rate (Hilburn
153 and Wentz 2008). The AMSR-E data are available from Remote Sensing System on a
154 0.25° × 0.25° grid (http://www.remss.com/). We use AMSR-E SST to locate the position
155 of the Gulf Stream front and use AMSR-E LWP to investigate the relationship between
156 LWP and LCT. CALIPSO, CloudSat and Aqua are three members of the A-train satellite
157 constellation that closely follow each other in orbit such and observe the same location
158 within 45 seconds. The nearly coincident measurements permit the combined analysis of
159 CALIPSO, CloudSat and AMSR-E.

160 In addition, DJF-averaged surface wind velocity and divergence are calculated from
161 daily QuikSCAT observations on a 0.25° × 0.25° grid (http://www.remss.com/; Liu 2002).
162 We calculate the DJF climatology to examine the pattern of surface wind
163 convergence/divergence associated with the Gulf Stream front.

164

165 *c. Reanalysis data*

166 We use the 6-hourly ERA-Interim fields on a 0.75° × 0.75° grid provided by the
167 European Center for Medium-Range Weather Forecasts (ECWMF, Dee et al. 2011).
168 ERA-Interim is the latest global atmospheric reanalysis to replace ERA-40. There are 12
169 vertical levels below 700 hPa, capable of characterizing MABL features across the SST

front. We use ERA-Interim at 0600 and 1800 UTC, which are close to the times of CALIPSO observations. The ERA-Interim fields are composited on LCT occurrence to investigate the MABL structure corresponding to the cross-frontal transition of low-level clouds.

d. Precipitation product

The Global Precipitation Climatology Project (GPCP) is used to depict the rainband associated with the Gulf Stream in DJF. We construct five-year (December of 2006-10, January and February of 2007-11) DJF-averaged precipitation based on daily GPCP data on a $1° \times 1°$ grid.

3. Winter climatology

The Gulf Stream flows along the North American coast, separates from the coast at Cape Hatteras and continues to flow northeastward. The sharp SST front between the warm Gulf Stream water and cold continental shelf water is most developed in winter (Minobe et al. 2010). Across the front, SST increases by 12 °C within 400 km, and the SST gradient is sharpest between 40 °N and 42 °N (Fig. 1).

Figure 1a shows that the Gulf Stream anchors a prominent rainband in winter on the southern side of the SST front. Precipitation in the rainband exceeds 7 mm day^{-1}, consistent with the results from the Tropical Rainfall Measuring Mission (Minobe et al. 2010). AMSR-E LWP also exhibits a cloud band over the warm water of the Gulf Stream,

191 collocated with the rainband (Fig. 1b). It should be noted that AMSR-E LWP excludes ice
192 clouds.

193 The formation of the rainband and cloud band is related to surface wind convergence
194 (Minobe et al. 2008) possibly via the sea level pressure (SLP) adjustment of Lindzen and
195 Nigam (1987). Low-level air temperature adjusts to an SST front through the
196 cross-frontal changes of sensible and latent heat flux, resulting in small-scale SLP
197 variations and upward motion over the warm flank of the SST front and high SLP and
198 downward motion over the cold flank. Minobe et al. (2010) found that the diabatic
199 heating and the upward motion over the warm water are confined to the lower
200 troposphere in winter, implying that the cross-frontal transition is more evident in
201 low-level clouds than higher clouds.

202 Indeed, the cross-frontal transition of LCT is sharp. Figure 2a and b show LCT
203 averaged within 0.5° intervals along the daytime and nighttime CALIPSO tracks over the
204 western North Atlantic during winter. Our composites include about 28 CALIPSO passes
205 along each track over the averaging period. LCT is lower than 1.4 km on the cold flank of
206 the SST front but rises to 2.4 km over the Gulf Stream. Along the 46°N latitude line
207 where the Gulf Stream flows northeastward, LCT is about 2.2 km at 40°W but only 1.4
208 km at 48°W, suggesting that the SST front exerts a strong influence on LCT. In general,
209 LCT is higher at night, indicative of a deeper MABL. This is because the entrainment is
210 strengthened by infrared radiation cooling at cloud top at night, but solar radiation
211 weakens this effect in the day. The enhanced entrainment helps deepen MABL (Caldwell,

2005). Further to the south away from the Gulf Stream, the gradual southward decrease of LCT from 35°N is due to large-scale subsidence of the subtropical high. For simplicity, we analyze CALIPSO and DARDAR data within the dashed quadrilaterals in which the Gulf Stream flows nearly eastward.

4. Composites of low-level cloud top

a. CALIPSO low-level cloud top

Figure 3a shows the zonally averaged DJF climatology of SST, SST minus surface air temperature (SST-SAT), meridional atmospheric circulation, and virtual potential temperature within the dashed quadrilaterals in Fig. 2. The SST front of the Gulf Stream is sharpest between 41-42.5°N (bottom panel of Fig. 3a) where the prevailing winds are westerly in winter. The westerly jet is 7.2 m s^{-1} at 38°N (not shown), and the meridional wind is weakly southerly over the SST front in the wintertime mean. The SST-SAT maxima are about 5.3 and 4.0 °C over the Gulf Stream and near 50°N (bottom panel of Fig. 3a), respectively. The former peak of SST-SAT is because the atmospheric adjustment to the SST front is slower than the increase of SST when the MABL is advected by the northerly wind from the cold to the warm water. The latter peak reflects the huge surface air temperature contrast between the ocean and continent in winter (Young and Sikora 2003). SST-SAT is an important parameter for lower-tropospheric stability and its spatial pattern is similar to the potential temperature difference between 700 hPa and 1000 hPa (not shown), an important parameter for the stratocumulus

233 formation (Wood 2012).

234 Although the large-scale motion is generally upward between 37-50°N, the
235 secondary circulation induced by the SST front is apparent (Fig. 3a). The ascending
236 motion is enhanced over the warm flank of the SST front and weakened over the cold
237 flank, with descending motion between 42 - 45°N below 2.0 km. This is consistent with
238 the surface convergence/divergence based on QuikSCAT (Fig. 1c) according to the
239 continuity equation. Such a secondary circulation in MABL is more evident after
240 applying spatial high-pass filtering (not shown).

241 Virtual potential temperature is relatively uniform in the vertical below 0.8 km,
242 indicative of a well-mixed MABL (the top panel of Fig. 3a). Closer examination suggests
243 that the MABL is shallower over the cold SST. The vertical gradient of virtual potential
244 temperature is greater between 1-1.5 km elevation on the cold flank of the SST front,
245 implying the frequent occurrence of temperature inversions capping MABL. Similarly,
246 near the Kuroshio Extension in winter, the near-surface instability (SST-SAT) effect on
247 the low-level atmospheric structure is obvious in observations (Tokinaga et al. 2009). The
248 lower atmosphere features a well-defined surface mixed layer under unstable condition,
249 whereas no surface mixed layer is observed in stable condition.

250 Figure 3b shows the relative frequency of LCT occurrence as a function of latitude
251 and altitude based on CALIPSO. In this case, the ERA-Interim fields (SST-SAT, vertical
252 and meridional winds, virtual potential temperature and the freezing level) are averaged
253 only when LCT is reported by CALIPSO. The relative frequency is calculated using 0.5°

254 bins in the meridional and 0.25 km bins in the vertical. ERA-Interim is interpolated along
255 the CALIPSO tracks in 0.5° meridional intervals. An ERA-Interim profile in a 0.5°
256 meridional bin contributes to the average if the bin contains at least 5 out of about 50
257 CALIPSO profiles that report LCTs.

258 The relative frequency of LCT occurrence exhibits large cross-frontal variations (Fig.
259 3b). The altitude with most frequent LCT is 1.3 km over the cold flank of the SST front
260 and rises to 1.8 km over the warm flank. Although an SST-SAT maximum and upward
261 motion occur between 48-50°N, LCT occurrence is less frequent since the air is dry near
262 the coast. CALIPSO is not able to detect the morphological categories of clouds, but
263 Norris and Iacobellis (2005) documented that stratocumulus is prevalent under cold
264 advection over SST gradient in the mid-latitude North Pacific. The relative frequency of
265 LCT gradually declines southward from 37°N where the MABL is much shallower,
266 suggesting the breakup of stratocumulus.

267 The cross-frontal cloud transition is related to the secondary atmospheric circulation
268 in the MABL induced by the SST front below 3 km (top panel of Fig. 3b). Downward
269 motion occurs below 3 km over the cold flank of the SST front. The frequent occurrence
270 of a temperature inversion over the cold SST confines most low-level clouds below 1.8
271 km. On the warm flank of the SST front, the composite upward motion is strongest at 2
272 km, consistent with the altitude of LCT occurrence. In contrast to the mean state (Fig. 3a),
273 stronger surface northerly wind occurs with LCT occurrence north of 40°N (Fig. 3b),
274 suggesting that the cross-frontal transition of low-level clouds is more prevalent under

surface northerlies. The composite surface northerly wind is strongest at the center of the SST front in agreement with the QuikSCAT results near the Kuroshio Extension (Tokinaga et al. 2009). Convergence of meridional surface wind over the warm SST is responsible for the ascending motion in the MABL.

Figure 4 further clarifies the cross-frontal transition of LCT, showing the probability density functions (PDFs) of transient LCT altitudes over the warm and cold water and their difference (warm minus cold). The regions of warm and cold water are defined as 0.5° bins centered at 40 and 45°N along the CALIPSO tracks, respectively. LCT is most frequent in 1.1-1.7 km over the cold SST but in 1.9-2.5 km over the Gulf Steam. About 50% of the time, the transient LCT at 40 °N is at least 0.5 km higher than at 45 °N. Similar results are obtained if we exclude all the profiles with clouds above 4 km (not shown).

The influence of the Gulf Stream on clouds might penetrate above the MABL and reach the mid-troposphere. The occurrence of cloud top above 4 km is more frequent over the warm water (not shown), supporting the results of Minobe et al. (2010) using Atmospheric Infrared Sounder and the Advanced Microwave Sounding Unit and Tokinaga et al. (2009) over the Western North Pacific. We focus on low-level clouds, however, since the cross-frontal transition below 4 km is more evident.

b. DARDAR cloud categories

Figure 5 shows cross-frontal transects of cloud phase categories from DARDAR. The

296 frequency of a cloud category occurrence is calculated using same bins as the relative
297 frequency of LCT occurrence. The altitude with the most frequent cloud occurrence
298 (about 60%) is 0.9 km over the cold flank of the SST front, and it reaches up to 1.7 km
299 over the warm flank, indicative of a cross-frontal structure. The categories of liquid and
300 rain dominate below 2.0 km over the warm water. Liquid clouds are more frequent above
301 1.2 km, while rain class is most frequent below 0.9 km over the Gulf Stream, supporting
302 the horizontal patterns of AMSR-E LWP and GPCP precipitation in winter (Fig. 1). In
303 contrast, ice clouds dominate above the freezing level. Ice clouds found above MABL in
304 the free troposphere (not shown) are due to storms. Additionally, the category of
305 supercooled liquid is mainly confined below 1.5 km over the cold flank of the SST front.
306 The categories of mixed ice and supercooled liquid are frequently observed near the LCT
307 and rise with the freezing level going southward. The SST front affects the freezing level
308 by transferring heat to the atmosphere and, therefore, influences the cross-frontal
309 variations of cloud categories.
310
311 *c. Relationship between CALIPSO LCT and AMSR-E LWP*
312 Figure 6 shows the joint PDFs of CALIPSO LCT and AMSR-E LWP over the warm
313 and cold flanks of the SST front, in the 0.5° bins centered at 40 and 45°N along
314 CALIPSO tracks, respectively. Assuming that most LWP is confined in the lower
315 atmosphere, it is plausible that larger LWP is associated with higher LCT due to greater
316 physical cloud thickness. This is consistent with the increase in LCT altitude with larger

LWP. As LWP increases from 0 to 0.08 mm, LCT increases by 0.8 km over the Gulf Stream (red contours) and by 0.3 km over cold water (blue contours), implying a higher correlation between LWP and LCT over warm water. The lower correlation over the cold water might be due to the frequent occurrence of ice clouds (Fig. 5) that are not included in AMSR-E LWP. Additionally, nearly all low clouds are confined below 2.5 km, which is the upper limit of the MABL in this region (not shown).

5. Northerly and southerly composites

Since the direction of the meridional surface wind is important for near-surface stability, the ERA-interim fields, the relative frequency of LCT occurrence, and frequencies of cloud categories are calculated separately for surface northerly and southerly regimes. Winds between 40-45°N are northerly (southerly) 54.7% (45.3%) of time, and the northerly and southerly composites include 55054 and 36170 LCT observations between 40-45°N, respectively.

a. Northerly wind composite

Figures 7a and 7b show the patterns of relative frequency of LCT and frequencies of different cloud categories under conditions of northerly wind reported at 10 m at the time and location of each satellite observation. These resemble the all-conditions composites (Figs. 3b and 5) since LCT occurs most frequently under northerly conditions. LCT is elevated over the Gulf Stream where SST-SAT exceeds 6.0 °C. Upon close inspection, the cross-frontal transition of relative LCT frequency is more evident than is the case in

338 the all-condition composites because of a stronger inversion produced by large-scale
339 subsidence over the cold flank of the SST front (Fig. 7a). Although the synoptic
340 northerlies are strong, the impact of the SST front on vertical motion is visible. The
341 large-scale descending motion is weakened over the warm flank of the SST front and
342 intensified over the cold flank. The strong surface northerlies lead to high SST-SAT, at
343 8.0 °C and 6.5 °C over the Gulf Stream and the coastal region (lower panel of Fig. 7a),
344 much higher than the mean-state and all-conditions composites (Figs. 3a and 3b). The
345 resulting MABL is more well-mixed under cold advection. Small et al. (2003) reported
346 that horizontal advection displaces the SAT response 100 km downwind of the SST
347 forcing in the region of Pacific tropical instability waves where the background winds are
348 approximately 10 m s^{-1}. A shorter length scale of the SAT adjustment to SST
349 perturbations is expected since the cross-frontal winds are 7 m s^{-1} in the northerly
350 composite.

351 In winter, the Gulf Stream front is under the North American Trough where the
352 prevailing winds are westerly (Fig. 8a) and is located in the storm track domain where the
353 synoptic variability is strong. In order to identify the specific synoptic conditions
354 corresponding to the cross-frontal transition of low-level clouds, the relative frequency of
355 LCT (not shown) and ERA-Interim (Fig. 8b) composites are constructed when the area
356 mean (between 40-45°N along the CALIPSO tracks) of surface meridional winds is
357 northerly. This calculation differs from Fig. 7a, which is composited on occurrence of
358 surface northerlies at the CALIPSO footprint. The relative frequency of LCT is similar to

359 the Fig. 7a (not shown), suggesting that the cross-frontal transition of low-level clouds is
360 robust. Figure 8b shows that cross-frontal northerlies related to the transition of low-level
361 clouds occur after low-pressure systems pass by. The resulting cold advection intensifies
362 heat and moisture flux out of the ocean to the atmosphere, and thus favors the formation
363 of stratocumulus (Young and Sikora 2003).
364
365 *b. Southerly wind composite*
366 Under southerly conditions, low-level clouds show more complex structures since
367 the entire atmosphere is influenced by synoptic large-scale ascent (Fig. 9a). In contrast to
368 northerly conditions, the MABL is stabilized by warm advection as warm air flows over
369 colder water. The most frequent LCT occurs near 37°N at 1.8 km and the maximum
370 frequency of rain category is collocated with large SST-SAT, although the near-surface
371 instability is much weaker than under northerly conditions (Fig. 9b). This suggests that
372 the Gulf Stream deepens clouds under the southerly flow and is consistent with the
373 argument of Norris and Iacobellis (2005) that precipitation and nimbostratus are more
374 frequent under regions of strong upward and poleward flow. There is a general northward
375 decrease in temperature in balance with the westerly thermal wind while the SST front
376 maintains a sharp temperature gradient near the surface. Compared to the northerly
377 composite, the freezing level is about 1 km higher at 40°N and occurs 5° poleward at 1
378 km altitude.
379

6. Seasonal cycle

The present study focused on the low-level cloud response to the Gulf Stream in winter when the SST front is sharpest, but low-level clouds vary markedly with seasons (Fig. 10). The seasonal variations of low-level clouds (Fig. 10) are closely related to the annual cycle of near-surface stability (Fig. 11). LCT is highest in winter and lowest in summer. In contrast to wintertime conditions, the strong southerly wind brings warm air over the relatively cold ocean during summer, thus stabilizing the surface layer. LCT frequently occurs below 1 km in summer, implying the frequent occurrence of sea fogs. These results based on CALIPSO are consistent with the visual observation from ships (Norris and Iacobellis 2005). Similarly, Li and Zhang (2013) observed a northward cross-SST-frontal transition from stratus to fog in the East China and Yellow Seas in summer. The relative frequency of LCT peaks over the SST front in winter but over the Gulf Stream in spring. This is because the Gulf Stream is the only heat source during cold-air outbreaks whereas SST-SAT is lower than 1 °C north of 43°N in spring (bottom in Fig. 10b) due to the weak springtime thermal contrast between the land and ocean (Young and Sikora 2003).

7. Summary and discussion

A sharp SST front develops between the warm Gulf Stream and cold continental shelf water during winter. We investigated the low-level cloud response to the SST front using CALIPSO and other high-resolution satellite observations and the ERA-Interim

401 reanalysis. The results show a strong southward cross-frontal elevation of low-level
402 clouds due to a secondary circulation within the MABL induced by the SST front.

403 The SST front exerts a strong influence on low-level clouds. Mean LCT averaged
404 along CALIPSO tracks is lower than 1.4 km over the cold flank of the SST front but
405 higher than 2.4 km over the Gulf Stream. In the zonal average, LCT over warm water is
406 0.5 km higher than over cold water. The SST front also influences the cross-frontal
407 variations of cloud phase categories by affecting the freezing level. Rain is the prime
408 form of precipitation over the Gulf Stream, ice clouds are dominant above the freezing
409 level, and supercooled clouds are frequently observed above the MABL over the cold
410 water in winter.

411 Our analysis supports the SLP adjustment mechanism proposed by Lindzen and
412 Nigam (1987) as an explanation for the secondary circulation within the MABL induced
413 by the SST front. The air temperature gradient within the MABL across the SST front
414 results in surface convergence and ascending motion over the Gulf Stream, consequently
415 deepening low-level clouds there.

416 The composite analysis shows that the cross-frontal transition of low-level clouds is
417 more evident when surface winds are northerly. Stronger northerly winds bring cold air
418 from the continent to the relatively warm ocean, leading to a well-mixed MABL that is
419 deeper over the southern flank of the SST front. Furthermore, synoptic subsidence
420 accompanying surface northerlies produces a strong inversion, thus setting up favorable
421 condition for the formation of low-level clouds.

Norris and Iacobellis (2005) investigated how mid-tropospheric vertical velocity and advection over the SST gradient control mid-latitude North Pacific cloud properties. They found that cumulus is prevalent under the conditions of synoptic descent and cold advection during winter and that the cloud breaks up as the MABL decouples when it is advected southward over the warmer water. Our results show that both the direction of surface meridional winds and the secondary circulation within the MABL induced by the SST front are important for the cross-frontal transition of low-level clouds. This is because the SST gradient in this study is much stronger than that in Norris and Iacobellis (2005).

Frequent and repeated observations by CALISPO make the results reported here more reliable than case studies. Our results illustrate the utility of CALISPO retrievals for air-sea interaction and MABL clouds in combination with AMSR-E and CloudSat. Further validation of the combined CALIPSO and CloudSat products (e.g., DARDAR) against in-situ observations is desirable.

Acknowledgments. The authors wish to thank Dr. L.-F. Sheng for her valuable comments. This work was completed while JWL was a visiting student at IPRC and Scripps sponsored by the China Scholarship Council. The data used in this study are obtained from the atmospheric scientific data center of NASA (CALIPSO), the ICARE Thematic Center (DARDAR-MASK), Remote Sensing Systems (AMSR-E, QuikSCAT), the ECMWF data server (ERA-Interim), and the Global Energy and Water Cycle

443 Exchanges Project (GPCP). This work is supported by the National Basic Research
444 Program of China (2012CB955602), NASA, the Natural Science Foundation of China
445 (41175006), and JAMSTEC. IPRC/SOEST Publication # xxx/yyy. J. R. Norris was
446 supported by NSF award AGS-0946094.
447

References

Bane, M., and E. Osgood, 1989: Wintertime Air-Sea Interaction Processes Across the Gulf Stream. *J. Geophys. Res.*, **94**, 10755–10772, doi: 10.1029/JC094iC08p10755.

Biswas, K. R., and P. V Hobbs, 1990: Lightning over the Gulf stream. *Geophys. Res. Lett.*, **17**, 941–943, doi: 10.1029/GL017i007p00941.

Bouniol, D., F. Couvreux, P.-H. Kamsu-Tamo, M. Leplay, F. Guichard, F. Favot, and E. J. O'Connor, 2012: Diurnal and seasonal cycles of cloud occurrences, Types, and radiative impact over West Africa. *J. Appl. Meteorol. Climatol.*, **51**, 534–553.

Caldwell, P, B. C. S., 2005: Mixed-layer budget analysis of the diurnal cycle of entrainment in southeast Pacific stratocumulus. *J. Atmos. Sci.*, **62**, 3775–3791.

Chelton, D., M. Schlax, M. Freilich, and R. Milliff, 2004: Satellite measurements reveal persistent small-scale features in ocean winds. *Science (80-.).*, **303**, 978–983.

Dee, D. P. and Coauthors, 2011: The ERA-Interim reanalysis: configuration and performance of the data assimilation system. *Q. J. R. Meteorol. Soc.*, **137**, 553–597.

Delanoë, J., and R. J. Hogan, 2008: A variational scheme for retrieving ice cloud properties from combined radar, lidar, and infrared radiometer. *J. Geophys. Res.*, **113**, D07204, 10.1029/2007JD009000.

Delanoë, J., and R. J. Hogan, 2010: Combined CloudSat-CALIPSO-MODIS retrievals of the properties of ice clouds. *J. Geophys. Res.*, **115**, D00H29, 10.1029/2009JD012346.

Delanoë, J., A. Protat, O. Jourdan, J. Pelon, M. Papazzoni, R. Dupuy, J.-F. Gayet, and C. Jouan, 2013: Comparison of Airborne In Situ, Airborne Radar–Lidar, and Spaceborne Radar–Lidar Retrievals of Polar Ice Cloud Properties Sampled during the POLARCAT Campaign. *J. Atmos. Ocean. Technol.*, **30**, 57–73.

Hilburn, K. A., and F. J. Wentz, 2008: Intercalibrated passive microwave rain products from the unified microwave ocean retrieval algorithm (UMORA). *J. Appl. Meteorol. Climatol.*, **47**, 778–794.

Hobbs, P. V, 1987: The Gulf Stream rainband. *Geophys. Res. Lett.*, **14**, 1142–1145, 10.1029/GL014i011p01142.

Huang, C.-Y., and S. Raman, 1988: A numerical modeling study of the marine boundary layer over the Gulf Stream during cold air advection. *Boundary-Layer Meteorol.*, **45**, 251–290.

Klein, S. A., and D. L. Hartmann, 1993: The seasonal cycle of low stratiform clouds. *J. Clim.*, **6**, 1587–1606.

Li, M., and S. Zhang, 2013: Impact of sea surface temperature front on stratus-sea fog over the Yellow and East China Seas — a case study with implications for climatology. *J. Ocean Univ. China*, **12**, 301–311.

Li, X., W. Zheng, and W. Pichel, 2004: A cloud line over the Gulf Stream. *J. Geophys. Res.*, **31**, 1–5, doi: 10.1029/2004GL019892.

Lindzen, R., and S. Nigam, 1987: On the role of sea surface temperature gradients in forcing low-level winds and convergence in the tropics. *J. Atmos. Sci.*, **44**, 2418–2436.

Liu, W. T., 2002: Progress in scatterometer application. *J. Oceanogr.*, **58**, 121–136.

Medeiros, B., L. Nuijens, C. Antoniazzi, and B. Stevens, 2010: Low-latitude boundary layer clouds as seen by CALIPSO. *J. Geophys. Res.*, **115**, D23, doi: 10.1029/2010JD014437.

Minobe, S., A. Kuwano-Yoshida, N. Komori, S.-P. Xie, and R. J. Small, 2008: Influence of the Gulf Stream on the troposphere. *Nature*, **452**, 206–209.

Minobe, S., M. Miyashita, A. Kuwano-Yoshida, H. Tokinaga, and S.-P. Xie, 2010: Atmospheric response to the Gulf Stream: Seasonal variations. *J. Clim.*, **23**, 3699–3719.

Nazaryan, H., M. P. McCormick, and W. P. Menzel, 2008: Global characterization of cirrus clouds using CALIPSO data. *J. Geophys. Res.*, **113**, D16, doi: 10.1029/2007JD009481.

Norris, J. R., 1998a: Low cloud type over the ocean from surface observations. Part I: Relationship to surface meteorology and the vertical distribution of temperature and moisture. *J. Clim.*, **11**, 369–382.

Norris, J. R., 1998b: Low cloud type over the ocean from surface observations. Part II: Geographical and seasonal variations. *J. Clim.*, **11**, 383–403.

Norris, J. R., and S. F. Iacobellis, 2005: North Pacific cloud feedbacks inferred from synoptic-scale dynamic and thermodynamic relationships. *J. Clim.*, **18**, 4862–4878.

O'Neill, L. W., D. B. Chelton, and S. K. Esbensen, 2010: The Effects of SST-Induced Surface Wind Speed and Direction Gradients on Midlatitude Surface Vorticity and Divergence. *J. Clim.*, **23**, 255–281.

Sampe, T., and S.-P. Xie, 2007: Mapping high sea winds from space: A global climatology. *Bull. Am. Meteorol. Soc.*, **88**, 1965–1978.

Sanders, F., 1986: Explosive cyclogenesis in the west-central North Atlantic Ocean, 1981--84. Part I: Composite structure and mean behavior. *Mon. Weather Rev.*, **114**, 1781–1794.

517 Sanders, F., and J. Gyakum, 1980: Synoptic-dynamic climatology of the “bomb.” *Mon.*
518 *Weather Rev.*, **108**, 1589–1606.

519 Small, R. J., S.-P. Xie, and Y. Wang, 2003: Numerical simulation of atmospheric
520 response to Pacific tropical instability waves. *J. Clim.*, **16**, 3723–3741.

521 Stein, T. H. M., D. J. Parker, J. Delanoë, N. S. Dixon, R. J. Hogan, P. Knippertz, R. I.
522 Maidment, and J. H. Marsham, 2011: The vertical cloud structure of the West
523 African monsoon: A 4 year climatology using CloudSat and CALIPSO. *J. Geophys.*
524 *Res.*, **116**, D22, 10.1029/2011JD016029.

525 Tokinaga, H., Y. Tanimoto, S.-P. Xie, T. Sampe, H. Tomita, and H. Ichikawa, 2009:
526 Ocean frontal effects on the vertical development of clouds over the Western North
527 Pacific: In situ and satellite observations. *J. Clim.*, **22**, 4241–4260.

528 Vaughan, M. a. and Coauthors, 2009: Fully automated detection of cloud and aerosol
529 layers in the CALIPSO lidar measurements. *J. Atmos. Ocean. Technol.*, **26**, 2034–
530 2050.

531 Wai, M. M.-K., and S. A. Stage, 1989: Dynamical analyses of marine atmospheric
532 boundary layer structure near the Gulf Stream oceanic front. *Q. J. R. Meteorol. Soc.*,
533 **115**, 29–44.

534 Winker, D. M., M. A. Vaughan, A. Omar, Y. Hu, K. A. Powell, Z. Liu, W. H. Hunt, and
535 S. A. Young, 2009: Overview of the CALIPSO mission and CALIOP data
536 processing algorithms. *J. Atmos. Ocean. Technol.*, **26**, 2310–2323.

537 Wood, R., 2012: Stratocumulus Clouds. *Mon. Weather Rev.*, **140**, 2373–2423.

538 Young, G. S., and T. D. Sikora, 2003: Mesoscale stratocumulus bands caused by Gulf
539 Stream meanders. *Mon. Weather Rev.*, **131**, 2177–2191.

540 Zhang, C., Y. Wang, A. Lauer, K. Hamilton, and F. Xie, 2012: Cloud base and top
541 heights in the Hawaiian region determined with satellite and ground-based
542 measurements. *Geophys. Res. Lett.*, **39**, D15, doi: 10.1029/2012GL052355.

543

544

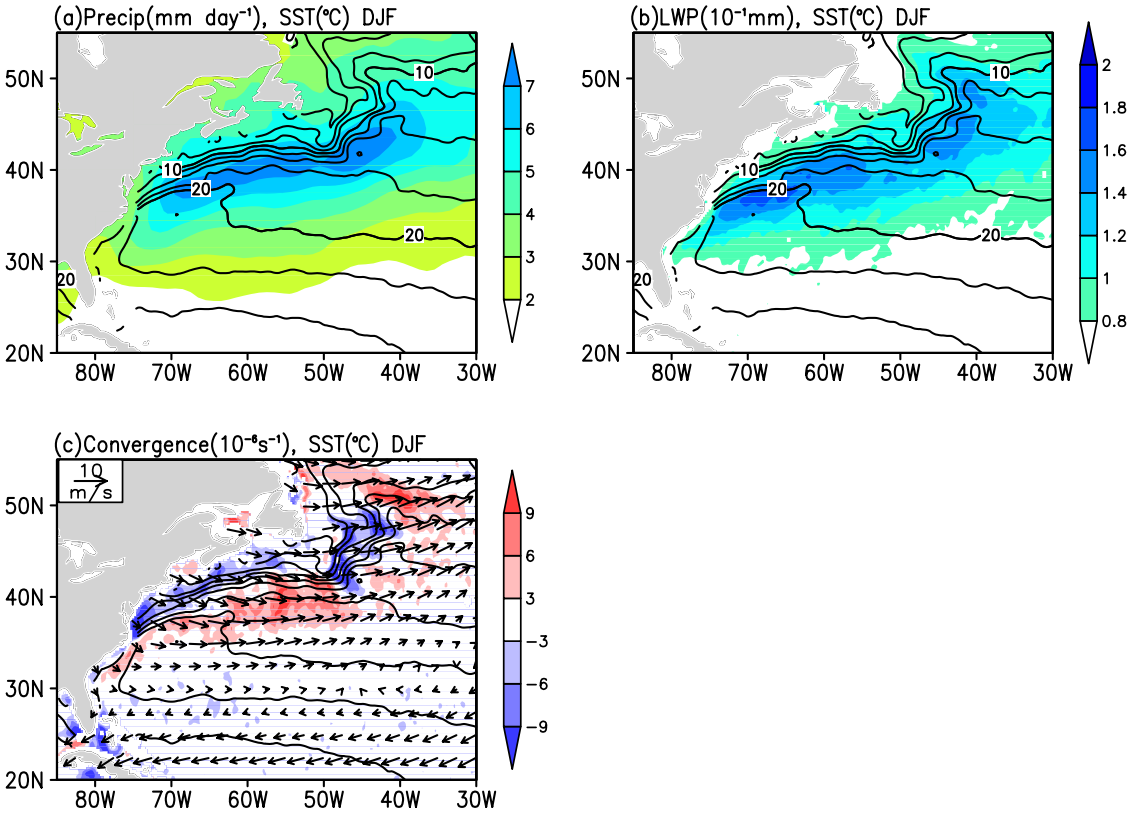

589

590 FIG. 1. DJF climatology: (a) GPCP precipitation (color shading in mm day^{-1}); (b) AMSR-E LWP

591 (color shading in mm); (c) QuikSCAT wind (vectors) and convergence (color shading in 10^{-5} s^{-1}).

592 AMSR-E SST [contours; contour intervals (CI) = 2°C] is superimposed.

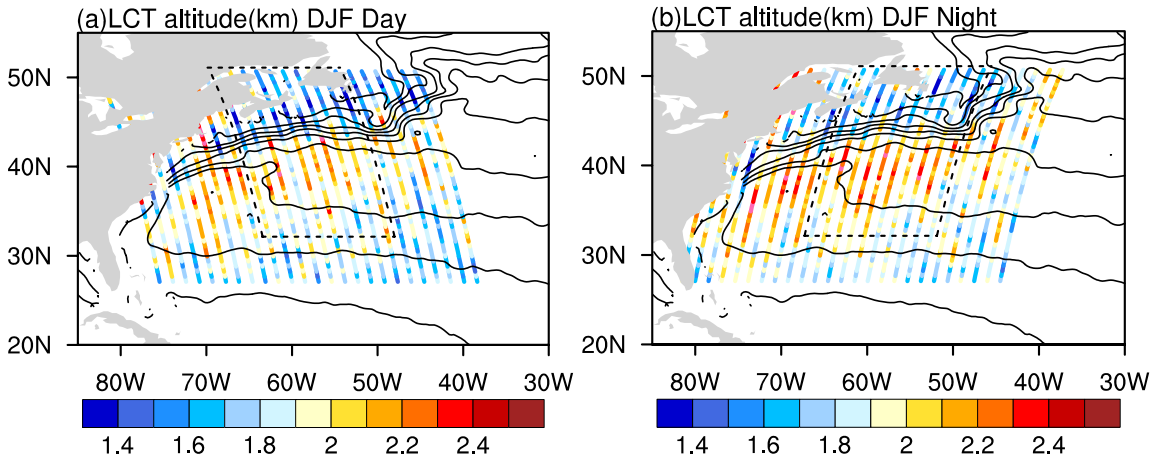

593

594 FIG. 2. DJF LCT altitude (color lines in km) along CALIPSO tracks during the day (a) and night (b)

595 with AMSR-E SST (contours; CI = 2°C) superimposed. The quadrilaterals indicate the spatial domain

596 of CALIPSO and DARDAR composites in subsequent figures.

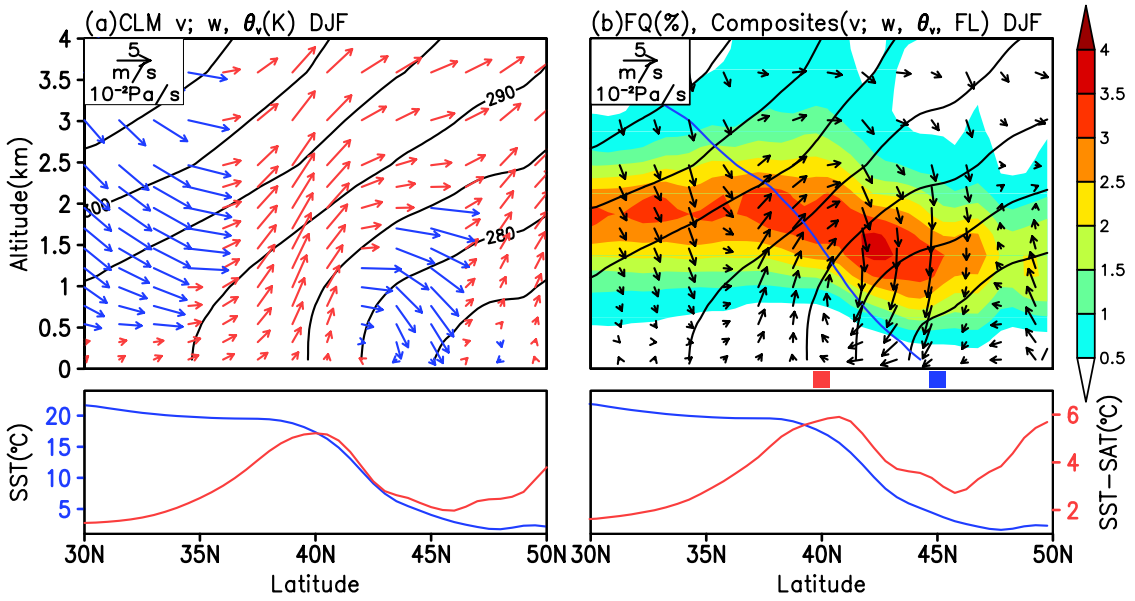

597

598 FIG. 3. (a) Zonal mean DJF climatology along CALIPSO tracks within the quadrilaterals in Fig. 2
599 from ERA-Interim: virtual potential temperature (contours; CI = 5 K), meridional wind (m s^{-1}) and
600 vertical velocity (10^{-2} hPa, vectors), SST (blue line in °C at bottom), and SST-SAT (red line in °C at
601 bottom). The red and blue vectors in the upper panel of (a) denote upward motion and downward
602 motion, respectively. (b) The relative frequency of LCT observed by CALIPSO as a function of
603 latitude and height (color shading in %). Composite virtual potential temperature (contours; CI = 5 K),
604 meridional wind (m s^{-1}) and vertical velocity (10^{-2} hPa, vectors) are constructed according to LCT
605 occurrence. The blue line in the top panel indicates the freezing level where the air temperature is 0
606 °C. The red and blue filled squares in Fig. 3b indicate the warm and cold regions used in Figs. 4 and 6.

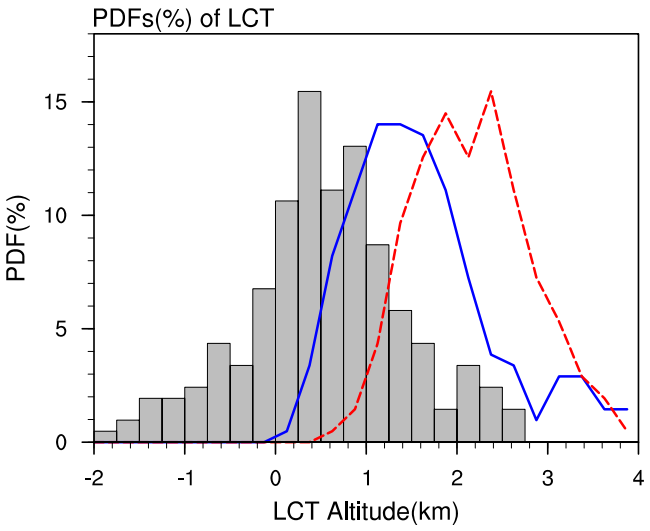

607

608 FIG. 4. PDFs (%) of LCT in two regions: 0.5° bins centered at 40 °N (red dashed line) and 45 °N (blue

609 solid line) along the CALIPSO tracks. The grey bars show the PDF of LCT differences between the

610 two regions (40 °N minus 45 °N) when the LCTs are observed in the two regions along one single

611 track.

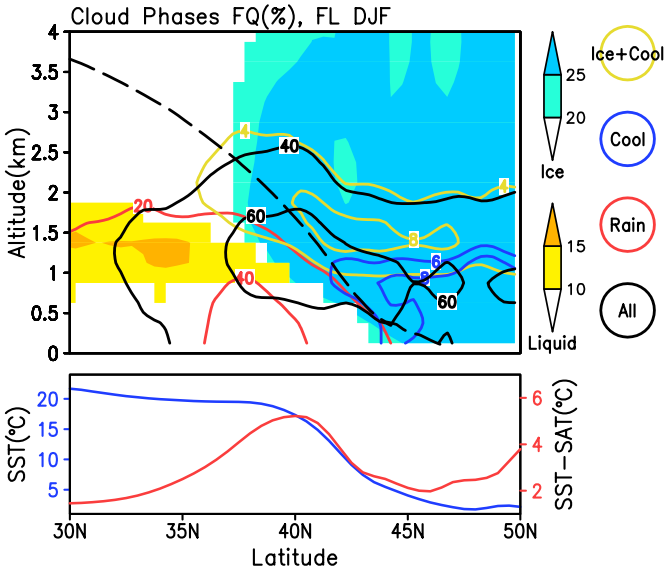

FIG. 5. Zonal mean of frequencies (%) of DARDAR cloud phases: all phases (black contours), ice (blue shading), liquid water (yellow shading), supercooled liquid water (blue contours), rain (red contours) and mixed ice and supercooled liquid water (yellow contours) clouds. The long dashed line indicates the freezing level. The blue and red lines in the bottom panel represent the same SST and SST-SAT in Fig. 3a, respectively.

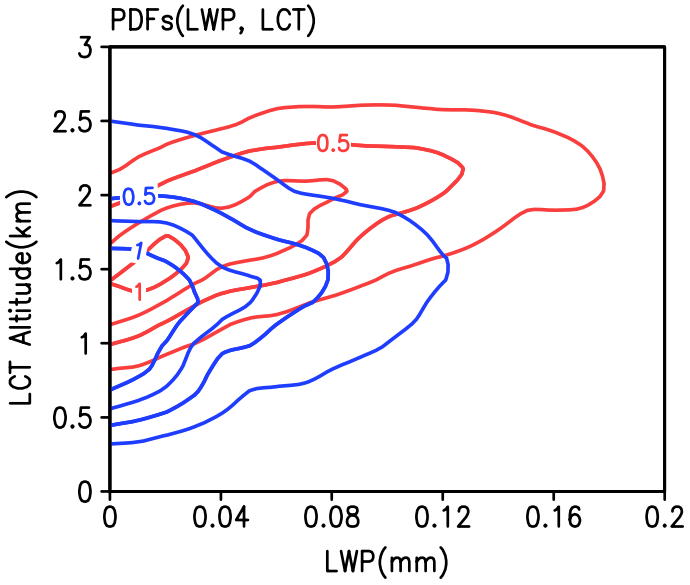

618

619 FIG. 6. Joint PDFs of LWP and LCT in two regions: 0.5° bins centered at 45°N (blue contours; CI =

620 0.25%) and 40°N (red contours; CI = 0.25%) along CALIPSO tracks.

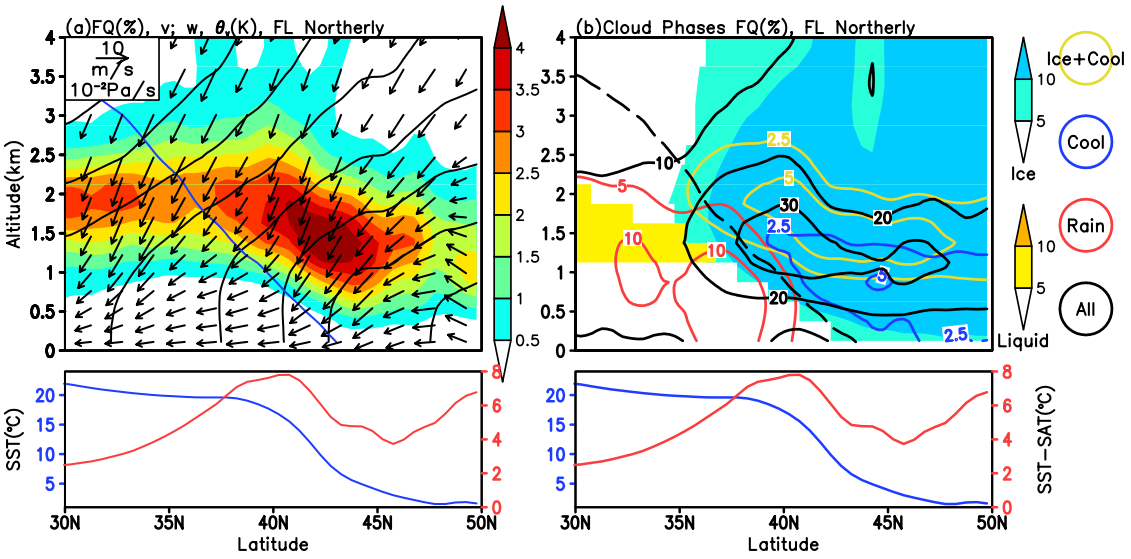

621

622 FIG. 7. (a) The relative frequency of LCT (color shading in %) and virtual potential temperature

623 (contours; CI = 5 K), meridional wind (m s^{-1}) and vertical velocity (10^{-2} hPa, vectors) under northerly

624 conditions are composited on the transient meridional surface winds along CALIPSO tracks. (b) As in

625 Fig. 5, but for composites under northerly and conditions according to meridional surface winds along

626 CALIPSO tracks.

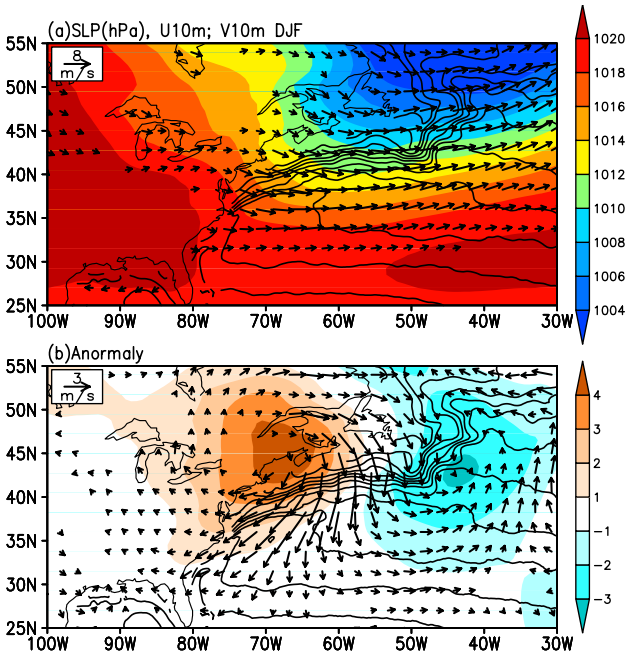

627

628 FIG. 8. (a) The DJF ERA-interim climatology: SLP (color shading in hPa), sea surface wind velocities

629 (vectors, m s^{-1}). (b) The composite anomalies of SLP (color shading in hPa), sea surface wind

630 velocities (vectors, m s^{-1}). The composites are constructed according to the occurrence of mean

631 northerly wind between 40-45°N along CALIPSO tracks. The wind speeds less than 2 m s^{-1} and 0.4 m

632 s^{-1} in (a) and (b) are omitted, respectively.

633

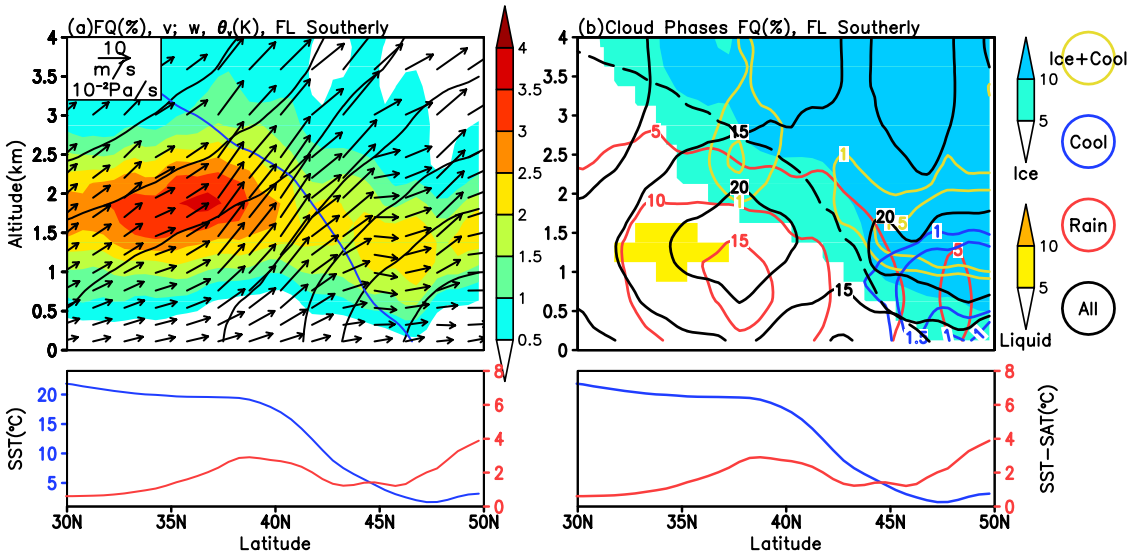

634

635 FIG. 9. As in Fig. 7, but for composites under southerly conditions.

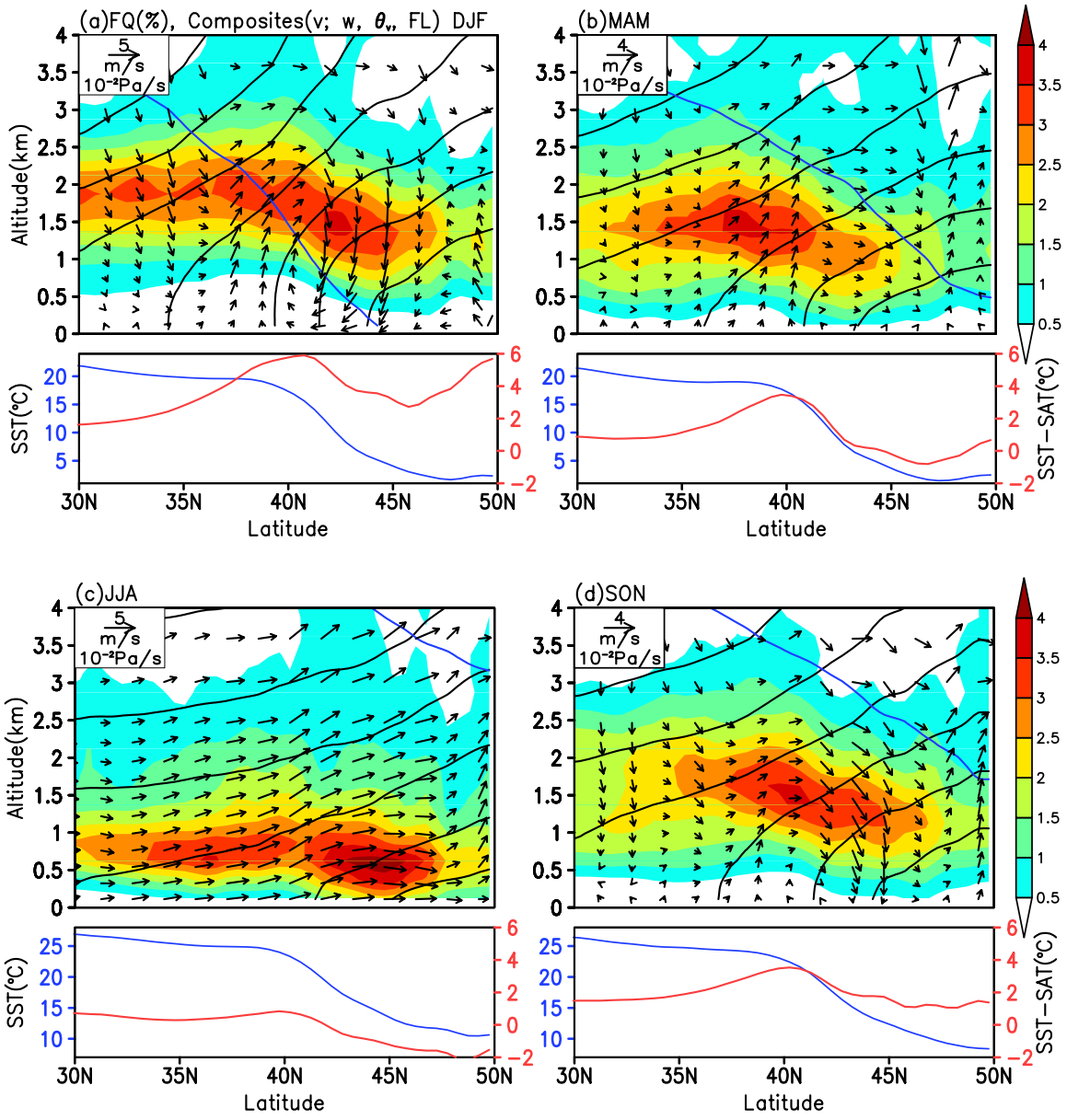

636

637

638 FIG. 10. (a) is identical to Fig. 3b. (b-d) are same as (a) but for MAM (b), JJA (c), and SON (d).

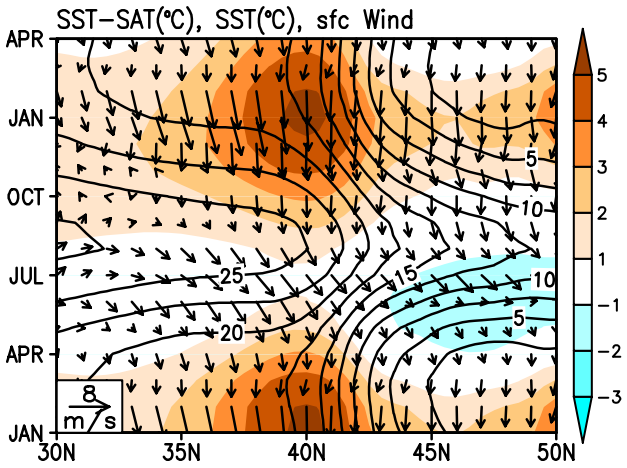

639

640 FIG. 11. Annual cycles of ERA-Interim SST (contours in °C), SST-SAT (color shading in °C) and

641 surface winds (vectors) that are zonally averaged ERA-Interim fields along CALIPSO tracks. The

642 horizontal and vertical components of the vectors represent the meridional and zonal surface winds,

643 respectively.

644